Mechanical Properties and Microstructural Characterization of Cu-4.3 Pct Sn Fabricated by Selective Laser Melting

ANTHONY P. VENTURA, C. AUSTIN WADE, GREGORY PAWLIKOWSKI, MARTIN BAYES, MASASHI WATANABE, and WOJCIECH Z. MISIOLEK

Components were fabricated *via* selective laser melting (SLM) of prealloyed Cu-4.3 pct Sn powder and heat treated at 873 K and 1173 K (600 °C and 900 °C) for 1 hour. Tensile testing, conductivity measurement, and detailed microstructural characterization were carried out on samples in the as-printed and heat-treated conditions. Optimization of build parameters resulted in samples with around 97 pct density with a yield strength of 274 MPa, an electrical conductivity of 24.1 pct IACS, and an elongation of 5.6 pct. Heat treatment resulted in lower yield strength with significant increases in ductility due to recrystallization and a decrease in dislocation density. Tensile sample geometry and surface finish also showed a significant effect on measured yield strength but a negligible change in measured ductility. Microstructural characterization indicated that grains primarily grow epitaxially with a submicron cellular solidification substructure. Nanometer scale tin dioxide particles identified *via* X-ray diffraction were found throughout the structure in the tin-rich intercellular regions.

I. INTRODUCTION

SELECTIVE laser melting (SLM) is an additive manufacturing technique based on powder bed fusion technology that can produce near fully dense metal components. In SLM, a laser guided by a computer model is used to fully melt metal powder on a build platform layer by layer until a fully functional component is produced. The key advantages of SLM include reduced development time, design freedom, and little material waste.[1] Copper alloys have seen extensive use with additive manufacturing as a binder or infiltrant, but rarely as a principle component to take advantage of their high conductivity properties.[2] Although some work exists on electron beam melting of commercially pure copper, there is relatively little available research on electrical grade copper alloy systems fabricated by SLM.[3,4] Copper alloys have been difficult to process *via* SLM due to the poor laser absorption of copper, but increases in laser power in commercial SLM units present the opportunity to fabricate high density copper alloy components.[5,6] Copper alloy components are of particular interest for electrical connector prototyping and fabrication of small production run components.

Numerous studies have been conducted on other metal alloys that demonstrate unique processing parameters inherent in SLM that affect microstructural characteristics and the resulting mechanical properties.[7,8] Of particular importance is the high cooling rate, which can be up to 10^8 K/s.[9] As a result of this high cooling rate, there is a significant chance for the formation of metastable phases or fine solidification substructure. For example, in Ti-6Al-4V, the resulting SLM microstructure is fine acicular martensitic.[10] Austenitic stainless steels, such as 316L, retain their austenitic structure, exhibiting solidification substructures with cell spacing on the order of 1 μm or less.[11] Additionally, intermetallic phases and nonmetallic particles have been found at the melt pool boundary, occasionally serving as initiation sites for cracking and failure. These particles include those that normally occur in the alloy during solidification/segregation as well as defects retained from the source powder or the SLM processing atmosphere.[10,12] Nearly all metallic alloys currently used in SLM exhibit epitaxial growth from the previous build layer, resulting in elongated grains in the build direction. Titanium alloys, in particular, exhibit very large columnar prior β grain boundaries, and conventional mill heat treatments do not produce optimum mechanical properties in SLM Ti-6Al-4V.[10,13] Studies on Ti-6Al-4V have also found that columnar grains formed from epitaxial growth have preferred growth directions that can vary throughout the cross section of the sample, and the morphology can be altered with the addition of in-process deformation steps.[14,15] Texture resulting

ANTHONY P. VENTURA, Loewy Graduate Fellow, MASASHI WATANABE, Associate Professor, and WOJCIECH Z. MISIOLEK, Loewy Professor and Chair, are with the Whitaker Lab, Materials Science and Engineering Department, Lehigh University, 5 East Packer Ave, Bethlehem, PA 18015. Contact email: apv211@lehigh.edu C. AUSTIN WADE, formerly Graduate Research Assistant with the Whitaker Lab, Materials Science and Engineering Department, Lehigh University, is now FEI Postdoctoral Research Fellow with the Materials Performance Centre, University of Manchester, Manchester, United Kingdom M13 9PL. GREGORY PAWLIKOWSKI and MARTIN BAYES, Principal Scientists, are with Tyco Electronics Corporation, a TE Connectivity Company, Harrisburg, PA 17111.

from directional solidification can be tailored with scanning strategy, as shown in an aluminum alloy as well as 316L stainless steel. Small changes in scanning complexity, for example, rotating the laser scan between build layers, were found to be sufficient to suppress strong texture development.[16,17]

Observations in the literature of the microstructural features present in SLM components are inherently focused on the particular physical metallurgy of the alloy being investigated. The research available on SLM does not address mechanical properties or microstructural characteristics of common copper alloy systems. The objectives of this research are to develop an understanding of an SLM copper alloy including the relationship between microstructural characteristics and mechanical properties as they develop during post-processing heat treatment. A binary Cu-4.3 pct Sn alloy was selected for this study as a simple model system to understand the general response of copper alloys to SLM.

II. EXPERIMENTAL METHODS

Prealloyed Cu-4.3 pct Sn gas-atomized powder was purchased from ECKA Granules with a maximum size of 63 μm. The powder was processed in an EOSINT M280 direct metal laser sintering unit with a 200 W Yb-fiber laser under a nitrogen atmosphere housed at TE Connectivity's Harrisburg, PA facility. A preliminary investigation was performed to determine the optimum laser parameters for maximum printed density measured by the Archimedes technique. Components were built on top of a support structure from a steel baseplate, and a standard raster scanning strategy with a 90-deg rotation between layers was employed. Along with the raster scanning, precontour and postcontour passes on the outer edge of each pass were completed. The interior volumes of the samples for this study were fabricated with a laser power of 195 W, a scan speed of 390 mm/s, a beam spot size of 190 μm, and a line spacing of 100 μm. The layer thickness was kept constant at 20 μm. The final density achieved with these settings was approximately 97 pct, as measured by the Archimedes technique and confirmed by light optical porosity measurements. Any further changes that resulted in higher total energy input, such as a finer laser spot or a slower scan speed, did not improve density beyond this point. These laser parameters were used to fabricate 1-mm-thick strip samples for conductivity measurement, all tensile samples, and 1-cm cubes for microstructural analysis.

Selected samples were postfabrication heat treated at 873 K and 1173 K (600 °C and 900 °C) in a sealed tube furnace under an argon atmosphere. The samples were heated at a rate of 15 K/min and held at the target temperature for 1 hour. After heat treatment, the samples were air cooled. Tensile testing was conducted on ASTM E-8 subsize rectangular specimens in the as-printed condition as well as CNC machined samples cut from overprinted rectangular prisms. The subsize rectangular tensile test samples had an overall length of

100 mm with 10-mm-wide grip sections and a reduced section 32-mm long by 6-mm wide. The filet radius between the grip section and reduced section was 6 mm. Uniaxial tensile tests were carried out on an Instron 5567 load frame with a 30-kN load cell, and samples were gripped with serrated mechanical wedge grips. Strain was determined by digital image correlation in conjunction with Bluehill 3 software and an Instron AVE2 video extensometer. Tensile specimens were loaded perpendicular to the build axis. Three samples of each condition were tested, and an average was taken for mechanical property reporting. The yield strength was calculated using the 0.2 pct offset method, and the elongation was taken as the strain at failure. Resistivity measurements were taken on $1 \times 1 \times 60$ mm^3 Cu-4.3 pct Sn strips (machined from larger printed sheets) using a four-wire method on a Keithley 580 Micro-Ohmmeter. Four samples were measured for each condition and averaged to determine the conductivity as a percentage of the International Annealed Copper Standard (pct IACS) based on the resistivity of pure annealed copper (172.41 $\mu\Omega$ cm).[18]

Printed cubes were sectioned using a Struers Accutom-50 high-speed abrasive cutoff wheel and mounted in cold-setting epoxy. Metallographic specimens were prepared using standard preparation techniques with a final attack polish (1 pct ammonium hydroxide, 1 pct hydrogen peroxide, and 98 pct, 0.05-μm colloidal silica) for light optical microscopy on a Reichart–Jung MeF3 optical microscope. Digital images were captured with a Nikon DxRi-1 camera and NIS Elements D software. Samples were etched in Klemm's I reagent. Vickers microhardness measurements were taken on etched metallographic samples with a Leco LM248AT using a load of 25 g. Electron backscatter diffraction (EBSD) was conducted on polished metallographic samples in a Hitachi 4300 field-emission scanning electron microscope. EBSD analysis was completed using TSL OIM analysis software, and the data were cleaned using grain dilation with a maximum of 9 pct of the collected points changed. A JEOL JXA 8900R electron probe microanalyzer (EPMA) was used to perform wavelength-dispersive spectroscopy analysis. Electron transparent specimens for (scanning) transmission electron microscope ((S)TEM) characterization were prepared by an FEI SCIOS focused ion-beam (FIB) instrument and were gently cleaned by using a Fischione 1040 Nanomill at 900 eV. TEM/STEM analysis, including X-ray energy dispersive spectrometry (XEDS), was completed using a JEOL JEM-ARM200CF aberration-corrected STEM. As-printed strip samples polished to 1 μm using standard metallographic preparation techniques were used for X-ray diffraction (XRD). XRD was completed on a PANalytical Empyrean unit with a Cu tube operating at 45 kV and 40 mA using Bragg–Brentano geometry. A $\theta:\theta$ scan was done for 2θ angles from 20 to 100 deg with a step size of 0.013 deg using a PIXcel3D-Medipix3 area detector in scanning line detector mode. Phi was varied from –30 to +30 deg to reduce any possible orientation effects, although no significant difference in the intensity of peaks between scans was observed. Peaks were

identified using PDXL software and the ICDD PDF-2 database.

III. RESULTS

A. *Physical Properties of Heat Treatments*

Prior to testing, tensile specimens were heat treated at 873 K and 1173 K (600 °C and 900 °C) for 1 hour. The lower temperature heat treatment represents a standard annealing heat treatment for typical bronze alloys.[18] The higher temperature heat treatment was chosen as a severe condition to induce significant microstructural change. Figure 1 shows the uniaxial tensile test results of 3-mm-thick SLM Cu-4.3 pct Sn in the as-printed condition as well as with the two heat treatments. All samples in Figure 1 were tested with the printed surface condition (*i.e.*, tensile bars were printed with dimensions that match ASTM E-8 subsize samples and tested with no alteration to the surface condition except removal of the support structure on one side). The physical properties of the SLM Cu-4.3 pct Sn are shown in Table I. The yield strength of the as-printed material is the highest with a value of 274 MPa. The heat-treated samples have lower yield strength values inversely related to the heat treatment temperature. The 873 K and 1173 K (600 °C and 900 °C) heat-treated samples have yield strengths of 208 and 102 MPa, respectively. Table I shows that the ultimate tensile strength values follow a similar trend. Ductility is the lowest in the as-printed sample at an elongation of 5.6 pct. Ductility increases with heat treatment temperature with values of 12.4 and 26.1 pct for the low- and high-temperature heat treatments, respectively. Although the total elongation has significant changes between the sample conditions, none of the samples exhibit any significant localized ductility after the ultimate tensile strength is reached. Conductivity measurements (Table I) show that the as-printed condition has the highest conductivity of 24.1 pct IACS, while the two heat-treated samples have similar conductivity values around 21 pct IACS. These values are in good agreement with wrought bronze alloys available commercially with similar tin concentrations.[18]

Figure 2 shows a light optical micrograph of the build direction of as-printed Cu-4.3 pct Sn. Individual weld pools from the SLM process can be seen running horizontally in Figure 2. Grains are elongated along the build direction, although their shape is highly varied. The grains also appear to stretch through multiple build layers. EPMA mapping showed a generally homogeneous distribution of tin throughout the material, with slight variations at the weld lines.

Figure 3 shows inverse pole figure (IPF) maps for SLM Cu-4.3 pct Sn in the as-printed and heat-treated conditions, obtained by EBSD. The maps more clearly show the elongated grain structure that was observed in Figure 2. In the as-printed condition, abnormally large grains as well as very fine grains can be found. However, most grains regardless of size tend to be elongated along the build direction. After the 873 K (600 °C) heat
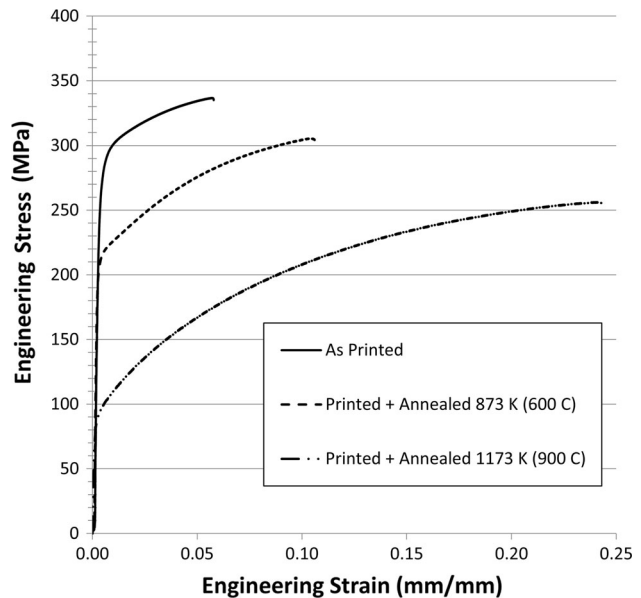

Fig. 1—Prototypical uniaxial tensile test results of SLM Cu-4.3 pct Sn in the as-printed condition as well as post-process heat treated at 873 K (600 °C) and 1173 K (900 °C).

treatment, there is little change in the grain morphology. After heat treatment at 1173 K (900 °C), the grain morphology has changed significantly, as shown in Figure 3(c). Grains are approximately equiaxed and contain annealing twins. Additionally, they are larger on average than in the other two conditions.

Figure 4 shows annular bright-field (ABF) STEM images of SLM Cu-4.3 pct Sn in the as-printed and two heat-treated conditions. The images show a high dislocation density in the as-printed condition as well as a moderate dislocation density in the printed and heat treated at 873 K (600 °C) sample. In contrast, the sample that underwent a heat treatment at 1173 K (900 °C) does not show an appreciable number of dislocations.

IV. DISCUSSION

A. *Grain Morphology*

The grain morphology observed in completed components is quite complex. Figure 2 shows many grains that extend through multiple build layers. In the bulk of the components (*i.e.*, away from the initial layers of the build), the molten metal is solidifying on top of previously solidified material of the same composition. As a result, there is complete wettability and the underlying layer acts as a nucleation site for solidification leading to epitaxial growth from lower layers similar to that commonly observed in autogenous welding and has been observed in SLM of other alloys.[10,14,16,19] In this experiment, there is a rotation of the laser scan direction between passes as well as the significant overlap and remelting in the build plane and between layers expected based on the build parameters. The direction of columnar growth is not entirely

Table I. Physical Properties of SLM Cu-4.3 Pct Sn in the As-Printed and Post-Process Heat Treated Conditions

Sample	Yield Strength (MPa)	Ultimate Tensile Strength (MPa)	Elongation at Failure (Pct)	Conductivity (Pct IACS)
As printed	274	334	5.6	24.1
Printed + annealed 873 K (600 °C)	208	309	12.4	21.2
Printed + annealed 1173 K (900 °C)	102	267	26.1	21.0
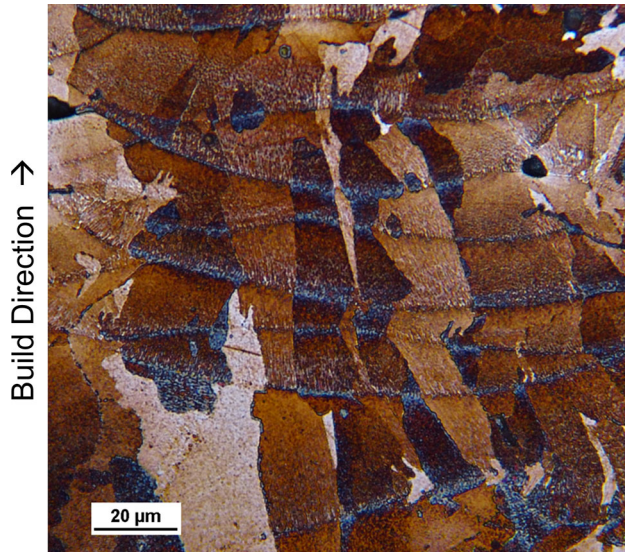
Fig. 2—Light optical micrograph of the build direction of as-printed Cu-4.3 pct Sn etched in Klemm's I reagent.

consistent throughout the material, as the direction of maximum heat extraction changes slightly during scanning in each individual weld pool. This is particularly noticeable in Figure 2 when grains change solidification direction abruptly along another (100) fast solidification direction at the weld line. However, the grains are all generally aligned along the build axis to a certain degree, as it is the common primary solidification direction. Although many grains clearly appear to have solidified epitaxially, it is also likely that heterogeneous nucleation mechanisms are active. There are a number of possible nucleation sites including but not limited to partially-melted adjacent powder particles, contamination in the weld pool (*e.g.*, oxide particles), and free surfaces. The significant amount of remelting makes it difficult to individually identify the secondary grain nucleation mechanisms, and epitaxial growth appears to be the dominant solidification mechanism. During solidification, competitive growth takes place, causing some grains to grow significantly larger and extend through multiple build layers while other grains are very fine, as shown in Figures 2 and 3.

Given the significant amount of remelting leading to epitaxial solidification and columnar grains, it is possible some texture would develop along the build direction. Figure 5 shows the EBSD IPFs taken from the transverse direction (IPFs are parallel to the build direction) of SLM Cu-4.3 pct Sn in the as-printed and two heat-treated conditions. No significant texture was

confirmed along the build direction in any of the sample conditions. Rotation of the laser-scanning direction appears to change the solidification conditions enough between different laser scans to inhibit a strong texture from developing. Similar observations have been reported in aluminum alloys.[16] However, the fields scanned to create these pole figures were held constant at 150 by 150 μm, leading to insufficient statistics to make definitive claims about the bulk texture of SLM Cu-4.3 pct Sn. A more detailed X-ray texture analysis is needed to fully understand the bulk texture of these samples.

B. *Effect of Geometry on Tensile Properties*

From a practical standpoint, it is useful to know if the mechanical properties measured in Figure 1 will be representative of small-scale electrical components fabricated from copper alloys *via* SLM. Figure 6 shows the uniaxial tensile testing results for samples tested under different surface and geometry conditions. The curve of the as-printed 3-mm-thick sample shown in Figure 6 corresponds to the as-printed curve in Figure 1 with a yield strength of 274 MPa. There are marked changes in yield strength and ultimate tensile strength based on the thickness of the tensile specimen as well as the surface conditions. The measured yield strength is the highest of 301 MPa for the case of a machined 3-mm-thick subsize tensile sample. The sample was machined down from a rectangular prism blank that was printed with a minimum of 1 mm of excess material on all sides. Additionally, samples in the as-printed condition with the same subsize geometry but a thickness of 1 mm have the lowest yield strength of 211 MPa. Using the 3-mm-thick as-printed condition as a baseline, there is a change of approximately $+10$ and -23 pct for the machined and 1-mm-thick as-printed samples, respectively.

Several studies have been conducted to investigate size effects during tensile testing as they pertain to making small components. In traditional wrought microstructures, during tensile testing, there is a general trend of decreasing strength as thickness decreases. This phenomenon is explained by the relationship of the grain size and the thickness of the specimens as well as the increased relative contribution from imperfections. As the number of grains spanning the cross section of the tensile specimen decreases, eventually, a significant portion of the grains are not constrained by the surrounding material, as is the case in thicker polycrystalline samples, leading to lower overall strength.[20] The critical thickness *vs* grain size varies for individual testing conditions. Work on aluminum and copper alloys has shown that for sheet with grain sizes on the
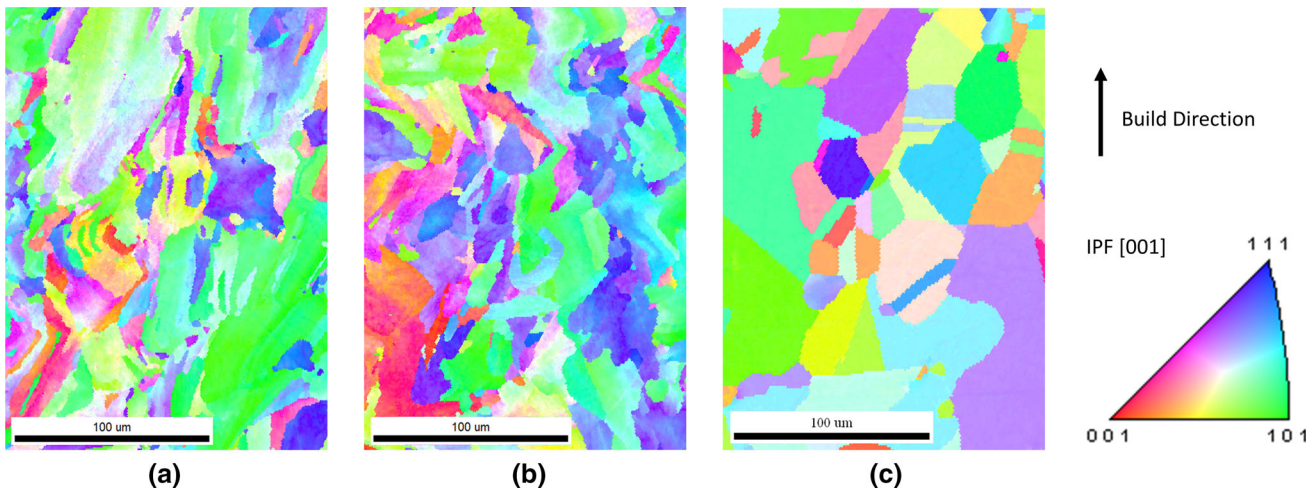
Fig. 3—IPF maps of SLM Cu-4.3 pct Sn in the (*a*) as-printed condition and after heat treatment at (*b*) 873 K (600 °C) and (*c*) 1173 K (900 °C).

order of 50 μm, the critical sheet thickness where the trend becomes noticeable is less than 1 mm.[20,21] Although it is difficult to directly apply this theory to the SLM structures observed in this study due to the unique grain morphology, observing the grain sizes from Figure 3(a) combined with a minimum specimen thickness of 1 mm suggests that the contribution of this mechanism is insignificant. This is further supported by the negligible change in ductility in Figure 6, which does not align with findings from wrought structures where the grain size/thickness effect was found to be active. Similarly, the effect of surface roughness was found to be relatively insignificant in the literature, particularly on samples thicker than 1 mm.[21]

Given the presence of porosity, oxide inclusions, and irregular grain morphology, the relative imperfection contribution is more likely to have a significant effect on the tensile properties of SLM materials. Of particular interest is porosity that tends to concentrate at the interface of the raster scan and the contours of the outside surface of the parts, which have been observed in this study approximately 50 to 100 μm from the surface. In the samples machined from a larger blank, this porosity band would be removed. In contrast, this porosity band would be more significant (*i.e.*, have a larger contribution related to the cross section of the gage length) in the 1-mm-thick as-printed samples. As a result, there is a significant variation in tensile properties reflected in Figure 6 based on sample condition, and this must be accounted for in component design.

### C. *Effect of Heat Treatment on Tensile Properties*

Figure 1 established the mechanical property dependence on heat treatment for SLM Cu-4.3 pct Sn for samples in the as-printed condition (no surface finishing) with a thickness of 3 mm. For electrical connectors, typically, the highest yield strength is desired to elastically store energy, thereby holding spring force in use. In the absence of required post-SLM forming operations (*e.g.*, bending to final part geometry), the ideal condition for use would be the as-printed condition. Regardless,

heat treatment has a significant effect on both the strength and ductility of SLM Cu-4.3 pct Sn.

Comparing the grain morphology in Figure 3 between the as-printed and 873 K (600 °C) heat-treated conditions indicates that there is no significant change between the two conditions. This implies that grain growth and the Hall–Petch relationship are not the dominant factors in the change in mechanical properties of the two conditions. Figure 4(a) shows a TEM image of the as-printed sample with a high dislocation density substructure. Although there is no deformation in the classical sense associated with the SLM process, significant thermal gradients and repeated heating and cooling cycles cause significant residual stresses.[22,23] As a result, the observed high dislocation density structure occurs, giving the as-printed condition the highest yield strength of the tested conditions. Additionally, the as-printed sample has a less pronounced strain hardening effect than the 873 K (600 °C) heat-treated sample. Despite the 873 K (600 °C) heat treatment being typical for wrought alloys of this type, recrystallization has apparently not occurred after 1 hour at this temperature.[18] Figure 4(b) shows qualitatively that the 873 K (600 °C) heat-treated sample still has a significant number of dislocations present in the structure, though less than in the as-printed condition. These observations combined with the tensile properties of the 873 K (600 °C) heat-treated sample suggest that some recovery has taken place and recrystallization may be occurring in discrete locations in the sample. Figure 7 shows a differential interference contrast light optical micrograph of the build direction of the 873 K (600 °C) heat-treated sample. Grains exemplifying the structure observed in Figure 3(b) can be found on the left half of the image, while a colony of equiaxed grains can be found on the right half. Microhardness measurements taken from six different fields show that the equiaxed grain colonies have an average hardness of 84 HV compared to an average of 123 HV for the surrounding grains that have similar morphology to the as-printed material. The equiaxed nature of the grains, the presence of annealing twins, as well as the lower microhardness
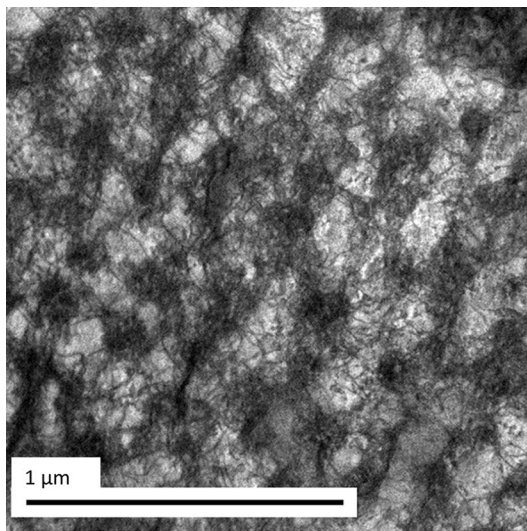
(a)
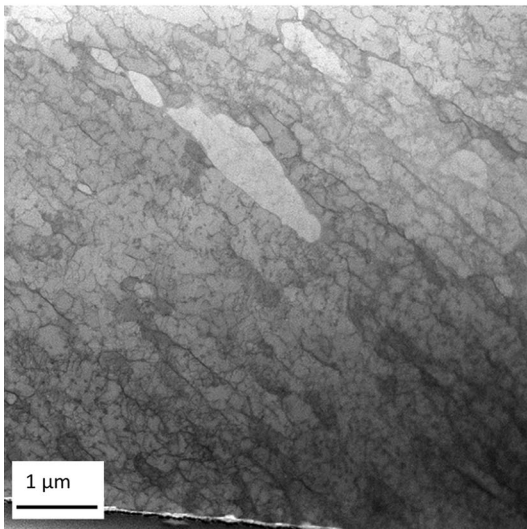
(b)
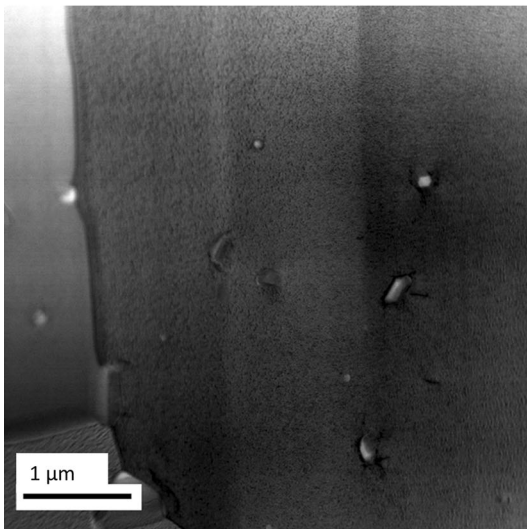
(c)

Fig. 4—ABF STEM microstructural comparison between SLM Cu-4.3 pct Sn in the (*a*) as-printed condition as well as printed and heat treated at (*b*) 873 K (600 °C) and (*c*) 1173 K (900 °C).

measurements from the grains indicate that they formed from recrystallization. The observed significant decrease in strength is not expected from a low stacking fault energy material, such as bronze, from recovery processes alone, which supports the hypothesis that the 873 K (600 °C) heat-treated sample underwent the initial stages of recrystallization.[24] The decreased number of dislocations in the sample and the discrete areas that have undergone recrystallization result in a lower yield strength and accompanying increase in ductility and strain hardening response. The 1173 K (900 °C) heat-treated samples have completed the recovery and recrystallization process. EBSD shows an equiaxed grain structure with a generally unimodal size distribution. Annealing twins can also be seen clearly within the grains. The structure would be expected to have a low dislocation density and the lowest strength of the sample conditions in this experiment. The structure is relatively dislocation free, as seen in Figure 4(c). With a larger grain size than the as-printed or 873 K (600 °C) heat-treated condition and a less dense network of dislocations, dislocation motion is not significantly impeded. The strength of this structure will be lower than the high dislocation density of the as-printed condition. The relatively large grained, low dislocation density structure of the 1173 K (900 °C) heat-treated sample has the lowest yield strength, highest ductility, and most dramatic strain hardening effect, as shown in Figure 1.

The overview of the mechanical properties in this study in Table I shows a wide range of attainable properties for SLM Cu-4.3 pct Sn. In relation to the mechanical properties, one of the largest effects of heat treatment is from alteration of the dislocation density in the material by way of recovery and recrystallization. The results indicate that heat treatments can be tailored to achieve desired properties, but the highest strength condition, in the case of the single-phase Cu-4.3 pct Sn alloy used in this study, is in the as-printed condition.

D. High-Magnification STEM and EDS

Weld lines characteristic of the SLM process can be clearly seen in Figure 2. Although weld lines could be resolved in the light optical images, EPMA compositional analysis did not indicate detailed inhomogeneity within the weld pools. The solidification substructure is apparently too fine to be resolved using light optical microscopy or EPMA. To examine the solidification substructure as well as the transition zone at the weld line, an electron transparent TEM specimen was extracted from a single grain across a weld line using an FIB instrument. This area of interest along the build direction of SLM Cu-4.3 pct Sn is shown in Figure 7. Areas rich in tin, verified *via* XEDS, are observed with a cellular morphology. Interestingly, the cell spacing appears to decrease as distance from the weld line increases. The findings are in agreement with the type of substructures found in SLM aluminum alloys.[16] Figure 8 also shows particles (dark spots) in the intercellular region. Based on the alloy composition, the microstructure is expected to be a single-phase
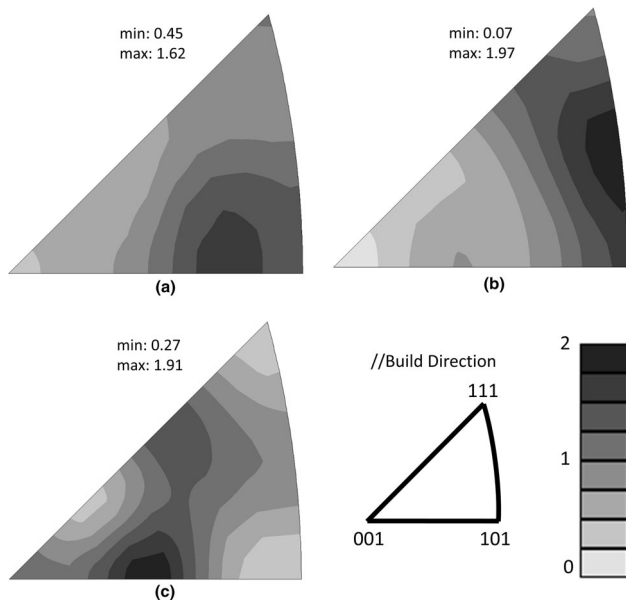
Fig. 5—IPFs taken from the transverse direction (parallel to the build direction) of SLM Cu-4.3 pct Sn in the (a) as-printed condition as well as heat treatment at (b) 873 K (600 °C) and (c) 1173 K (900 °C).
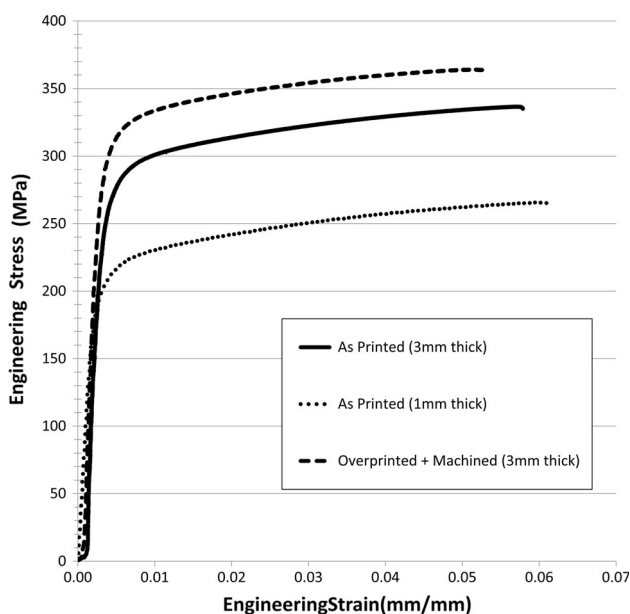

Fig. 6—Prototypical uniaxial tensile test results of SLM Cu-4.3 pct Sn in the as-printed condition 3-mm thick and 1-mm thick and a sample that was machined from a rectangular prism to 3-mm thickness.

face-centered-cubic (fcc) solid solution with no second-phase particles. Figure 9 shows a high-magnification BF STEM image of one of the particles from the as-printed condition along with XEDS intensity maps of copper, oxygen, and tin. The particles show a high intensity of tin and oxygen compared to the surrounding matrix phase. There is negligible copper intensity within the particle, indicating that the particles are some type
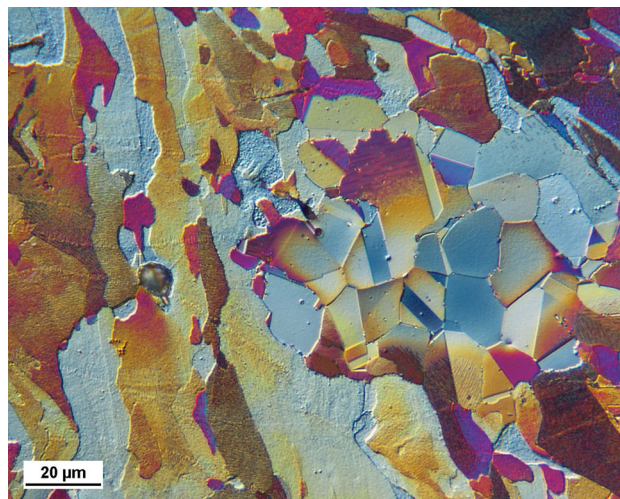
Fig. 7—Differential interference contrast light optical micrograph of the build direction of SLM Cu-4.3 pct Sn heat treated at 873 K (600 °C) etched in Klemm's I reagent.
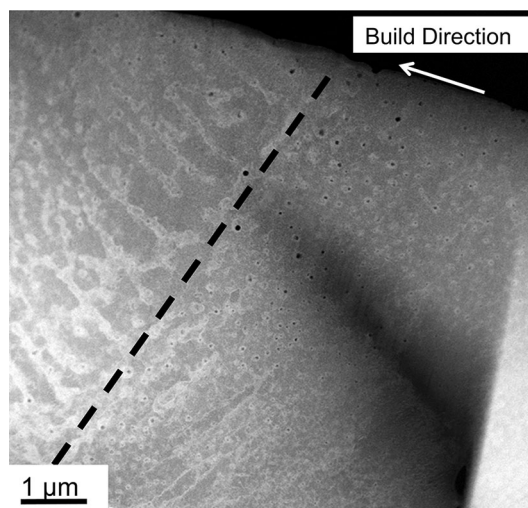
Fig. 8—ABF STEM image along the build direction of as-printed SLM Cu-4.3 pct Sn showing an individual weld line (dashed line) and solidification substructure.

of tin oxide, likely due to the relatively high affinity of tin to form tin oxide compared to copper.[25] Figure 10 shows XRD results of the as-printed SLM Cu-4.3 pct Sn. Peaks from the fcc copper matrix (with tin in solid solution) are identified along with peaks corresponding to the oxide particles, which indicate that the particles are SnO_2. The particles are approximately 40 to 60 nm in diameter and homogeneously distributed through the specimen on a large scale, although they are typically confined to the intercellular regions locally. The particles are likely introduced from oxide on the surface of the precursor powder given the low oxygen build atmosphere that is flushed with argon in the EOSINT M280 used for this experiment. During solidification, tin and oxygen that are dissolved in the copper are expected to be segregated into the intercellular regions simultaneously due to constitutional supercooling. Upon

reaching a critical temperature, the SnO_2 is expected to form during solidification.

After heat treatment at 873 K (600 °C), the oxide particles do not have a significant change in morphology. Although evidence of the cellular substructure is eliminated, the size and distribution of the oxide particles do not noticeably change, as shown in Figure 11. The oxide particles are small enough to interact with dislocations in the as-printed and 873 K (600 °C) heat-treated sample, suggesting that they may be acting as strengthening particles as in oxide dispersive-strengthened alloys. Additionally, the oxide particles may be interfering with recovery and recrystallization, thereby explaining the limited response of the material to the 873 K (600 °C) heat treatment. Due to the significant microstructural changes during heat treatment of the samples in this study, a definitive contribution to strength from the oxide particles could not be established.

After heat treatment at 1173 K (900 °C), the oxide particles coarsened significantly to sizes that are unlikely to significantly enhance strength, as seen in Figure 12. There is a wide range of particle sizes in the 1173 K (900 °C) heat-treated sample, with particularly large particles along grain boundaries and at triple points. The oxide
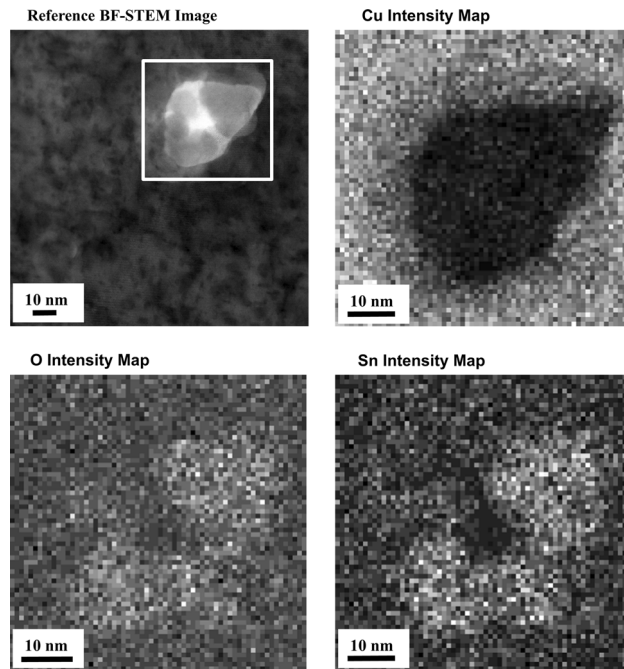

Fig. 9—BF-STEM and accompanying XEDS intensity maps of typical small particles observed in the intercellular regions of the as-printed Cu-4.3 pct Sn.
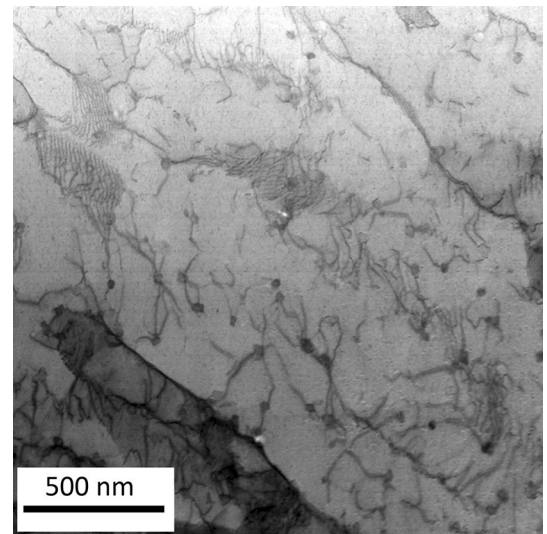

Fig. 11—ABF-STEM image of oxide particles (dark spots) observed in SLM Cu-4.3 pct Sn heat treated at 873 K (600 °C).
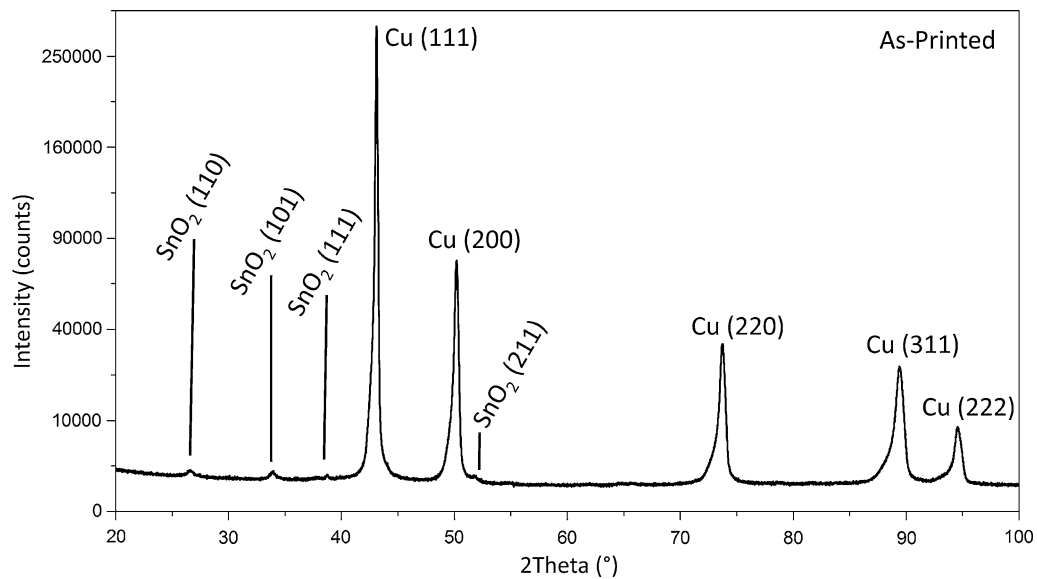

Fig. 10—XRD pattern obtained from as-printed SLM Cu-4.3 pct Sn.
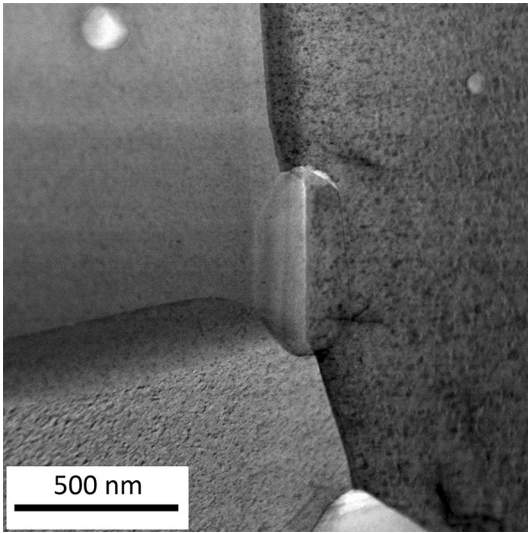
Fig. 12—BF-STEM image of oxide particles observed in SLM Cu-4.3 pct Sn heat treated at 1173 K (900 °C).

coarsening is consistent with an Ostwald ripening mechanism wherein small particles are sacrificially dissolved as large particles grow. Particles on boundaries grow larger due to the enhanced diffusion along grain boundaries.[26] Based on the qualitative observations of dislocation density from TEM analysis, the conductivity would be expected to increase with heat treatment.[18] However, conductivity was highest in the as-printed condition. The changes in conductivity between the sample conditions described in Table I are likely a result of the oxide particle coarsening process. During heat treatment, tin and oxygen atoms from smaller particles are dissolved back into the matrix and diffuse along a concentration gradient between particles of different sizes resulting from the Gibbs–Thomson effect.[26] Although the larger particles are growing, the local solute concentration in the matrix increases in relation to the as-printed condition because of the sacrificial dissolution of smaller particles. Solute atoms in the matrix have a significant effect on the conductivity of copper alloys, resulting in a decrease in conductivity that outweighs the contribution from a lower dislocation density structure.[18] In other words, solute atoms (oxygen and tin in this case) are more influential than lowering the dislocation density, thereby degrading the conductivity.

V. CONCLUSIONS

The mechanical properties of selective laser-melted Cu-4.3 pct Sn during post-processing heat treatment were investigated in conjunction with microstructural characterization. Samples were fabricated for analysis in the as-printed condition as well as heat treated at 873 K and 1173 K (600 °C and 900 °C). Uniaxial tensile tests and electron microscopy techniques were used to characterize the resultant microstructure and properties of each condition. The following conclusions were reached as a result of this work pertaining to SLM Cu-4.3 pct Sn:

1. Optimization of build parameters, namely, the laser power and beam focus, resulted in part densities around 97 pct. The primary grain growth mechanism is epitaxial growth, and there is a cellular solidification substructure with submicron spacing.
2. The as-printed condition has the highest yield strength and conductivity measured (274 MPa, 24.1 pct IACS) but the lowest ductility (5.6 pct elongation).
3. Heat treatment reduces the yield strength and increases the ductility markedly, primarily as a result of recrystallization and a decrease in dislocation density.
4. Tensile sample geometry and surface finish have a significant effect on the measured tensile properties and must be taken into account during design and processing.
5. High-resolution STEM analysis reveals nanometer scale tin dioxide particles throughout the structure in the tin-rich intercellular regions.

REFERENCES

1. I. Gibson, D. Rosen, and B. Stucker: *Additive Manufacturing Technologies*, 1st ed., Springer, New York, 2010, p. 459.
2. J.P. Kruth et al.: *Rap. Prototyp. J.*, 2005, vol. 11 (1), pp. 26–36.
3. D. Ramirez et al.: *Acta Mater.*, 2011, vol. 59 (10), pp. 4088–99.
4. M. Lodes, R. Guschlbauer, and C. Körner: *Mater. Lett.*, 2015, vol. 143, pp. 298–301.
5. N. Tolochko et al.: *Rap. Prototyp. J.*, 2000, vol. 6 (3), pp. 155–61.
6. S. Pogson et al.: *Rap. Prototyp. J.*, 2003, vol. 9 (5), pp. 334–43.
7. D. Gu et al.: *Int. Mater. Rev.*, 2012, vol. 57 (3), pp. 133–64.
8. B. Song et al.: *Front Mech. Eng.*, 2015, vol. 10 (2), pp. 111–25.

9. L. Loh *et al.*: *Int. J. Heat Mass Transfer*, 2015, vol. 80, pp. 288–300.
10. L. Thijs *et al.*: *Acta Mater.*, 2010, vol. 58 (9), pp. 3303–12.
11. E. Yasa and J.P. Kruth: *Proc. Eng.*, 2011, vol. 19, pp. 389–95.
12. W. Shifeng *et al.*: *J. Mater. Process. Technol.*, 2014, vol. 214 (11), pp. 2660–67.
13. B. Vrancken *et al.*: *J. Alloys Compd.*, 2012, vol. 541, pp. 177–85.
14. A.A. Antonysamy *et al.*: *Mater. Charact.*, 2013, vol. 84, pp. 153–68.
15. J. Donoghue *et al.*: *Mater. Charact.*, 2016, vol. 114, pp. 103–14.
16. L. Thijs *et al.*: *Acta Mater.*, 2013, vol. 61 (5), pp. 1809–19.
17. T. Niendorf *et al.*: *Metall. Mater. Trans. B*, 2013, vol. 44B, pp. 794–96.
18. J. Davis: *ASM Specialty Handbook: Copper and Copper Alloys*, 1st ed., ASM International, Materials Park, OH, 2001, pp. 3–5 and 32–50.
19. S. Kou: *Welding Metallurgy*, 1st ed., Wiley, Hoboken, NJ, 2003, p. 478.
20. T. Kals and R. Eckstein: *J. Mater. Process. Technol.*, 2000, vol. 103 (1), pp. 95–101.
21. C.H. Suh, Y.C. Jung, and Y.S. Kim: *J. Mater. Sci. Technol.*, 2010, vol. 24 (10), pp. 2091–98.
22. B. Vrancken *et al.*: *Solid Freeform Fabrication Symp. Proc.*, 2013, pp. 393–407.
23. P. Mercelis and J.P. Kruth: *Rap. Prototyp. J.*, 2006, vol. 12 (5), pp. 254–65.
24. H. McQueen and W.J M. G Tegart: *Sci. Am.*, 1975, vol. 232 (4), pp. 116–25.
25. H. Ellingham: *J. Soc. Chem. Ind.*, 1944, vol. 63 (5), pp. 125–60.
26. D. Porterling and K. Easterling: *Phase Transformations in Metals and Alloys*, 3rd ed., FL, Boca Raton, 2009, pp. 100–04.